Probe-configuration-dependent dephasing in a mesoscopic interferometer

G. Seelig, S. Pilgram, A. N. Jordan, and M. Büttiker

Département de Physique Théorique, Université de Genève, CH-1211 Genève 4, Switzerland

(Received 19 August 2003; published 23 October 2003)

Dephasing in a ballistic four-terminal Aharonov-Bohm geometry due to charge and voltage fluctuations is investigated. Treating two terminals as voltage probes, we find a strong dependence of the dephasing rate on the probe configuration in agreement with a recent experiment by Kobayashi, Aikawa, Katsumoto, and Iye [J. Phys. Soc. Jpn. **71**, 2094 (2002)]. Voltage fluctuations in the measurement circuit are shown to be the source of the configuration dependence.

Recently, Kobayashi, Aikawa, Katsumoto, and Iye[1] measured the reduction of the Aharonov-Bohm (AB) effect[2] in a ballistic four-terminal ring due to decoherence and thermal averaging. Not only was the visibility of the AB oscillations found to be much larger in the nonlocal configuration (see Fig. 1), but also decoherence was observed to be considerably weaker than in the local configuration (see Fig. 1). That the external measurement circuit can strongly influence the physical properties of a mesoscopic conductor has been shown for a variety of problems ranging from dephasing in disordered conductors[3] to Coulomb blockade[4] or the higher moments of the noise in a tunnel junction.[5] However, to the best of our knowledge the experiment of Kobayashi *et al.*[1] provides the first experimental evidence of such a striking dependence of the coherence properties of open mesoscopic conductors on the *measurement configuration*. Such a measurement circuit is part of every conductance measurement and it is therefore important to provide a theoretical explanation of this phenomenon.

In the experiment,[1] the decoherence rate was extracted from a measurement of the four-terminal resistance $R_{\alpha\beta,\gamma\delta}$. The two contacts α,β are voltage biased and monitored by an ammeter while the two contacts γ,δ are connected to a voltmeter. In mesoscopic transport, the four-probe character of resistance measurements[6] becomes apparent if the probes are within a coherence volume of the sample.[7] A resistance measurement is termed *local* if the voltage probes are along the current path and is termed *nonlocal* if the voltage probes are far from the current path. For the conductor shown in Fig. 1, $R_{14,23}$ is a local resistance, whereas $R_{12,34}$ is an example of a nonlocal resistance. We emphasize that the sample is the same, independent of the resistance measured: what changes is how the sample is connected to the current source and to the voltmeter.

AB oscillations are the result of quantum interference from electrons traveling through the two arms of the ring. In ballistic mesoscopic rings these oscillations can be larger than 50% of the total current amplitude,[1,8,9] and their decay is a measure of decoherence in the system (once thermal averaging is taken into account). Experimental investigations[10,11] found a linear temperature dependence of the dephasing rate.[11] A theoretical explanation, starting from fluctuating electrostatic potentials in the ring, is given in Ref. 12. Similar results for the temperature dependence of the dephasing rate, both experimental[13,14] and theoretical,[15] have

been obtained previously for chaotic quantum dots. Here, we are concerned with another feature of the dephasing rate, namely, its probe-configuration dependence.[1]

First, we illustrate our approach for a (reflectionless) electronic Mach-Zehnder interferometer (MZI).[12] In a second step, we consider interferometers with backscattering at the intersections. In both cases, the arms of the ring are treated as perfect one-channel leads that can be charged up relative to nearby side gates via the capacitances C_A and C_B. The setup is sketched in Fig. 1. For the MZI, the intersections are described as reflectionless beam splitters (see inset in Fig. 2) with a scattering matrix

$$\mathbf{S}_B = \begin{pmatrix} 0 & \mathbf{s} \\ \mathbf{s} & 0 \end{pmatrix}, \quad \mathbf{s} = \begin{pmatrix} \sqrt{\mathcal{T}} & i\sqrt{1-\mathcal{T}} \\ i\sqrt{1-\mathcal{T}} & \sqrt{\mathcal{T}} \end{pmatrix}. \quad (1)$$

Here, $\sqrt{\mathcal{T}}$ is the amplitude for going straight through the intersection and $i\sqrt{1-\mathcal{T}}$ the amplitude for being deflected. Due to the absence of backscattering, the MZI does not exhibit closed electronic trajectories.

Electron-electron interactions give rise to fluctuations of the internal potentials $U_i(t)$ ($i=A,B$). In the presence of interactions, the dimensionless conductance G_{13} relating current at contact 1 to a voltage applied to contact 3 is[12]
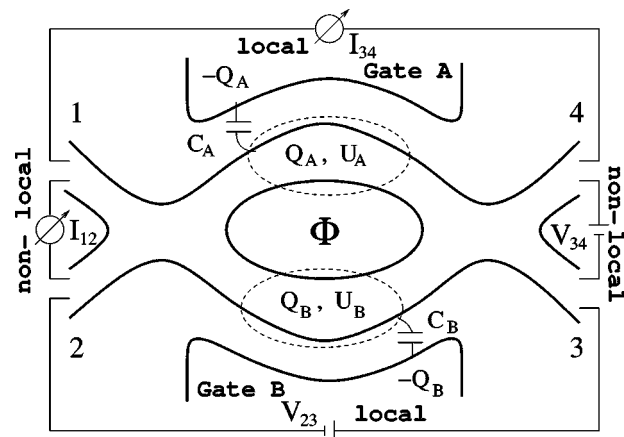

FIG. 1. Ballistic four-terminal ring: An internal potential $U_i(t)$ and a charge $+Q_i(t)$ belong to each arm of the ring ($i=A,B$). Each arm is coupled to a side gate via a capacitance C_i. The local and nonlocal probe configurations are indicated.
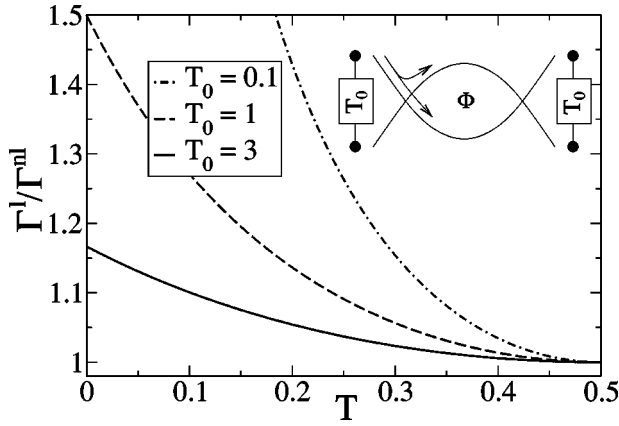
FIG. 2. The ratio of the local to the nonlocal decoherence rate is shown as a function of the transmission $\mathcal{T}$ at the beam splitters for different values of the incoherent parallel resistance $1/T_0$. All curves are symmetric with respect to $\mathcal{T}=1/2$. In the inset, the two possible electron paths at the beam splitter and the resistance $1/T_0$ (in units of h/e^2) are indicated.

$$G_{13}= -\langle T_{13}\rangle= -2\mathcal{T}(1-\mathcal{T})[1+e^{-\tau\Gamma_\phi}\cos(2\pi\Phi)]. \quad (2)$$

Here, T_{13} is the transmission probability, $\tau=L/v_F$ is the traversal time, Φ is the magnetic flux through the ring (in units of the flux quantum), and we have taken equal arm lengths in the ring, $L_A=L_B=L$. The angular brackets denote an average over the potential fluctuations in the ring.[16] In the limit of classical Nyquist noise, the decoherence rate

$$\Gamma_\phi=\frac{e^2}{2\hbar^2}\Sigma_{UU}(0) \quad (3)$$

is proportional to the spectral function $\Sigma_{UU}(0)$ of the potential difference $U(t)=U_A(t)-U_B(t)$ in the zero-frequency limit. If all four contacts are connected to a zero-impedance external circuit kept at constant voltage, the rate Γ_ϕ of dephasing due to (small energy transfer) electron-electron scattering is

$$\gamma_\phi^0=\frac{2kTe^2}{\hbar^2}\left(\frac{C_\mu}{C}\right)^2 R_q. \quad (4)$$

Here, T is the temperature, $R_q=h/(4e^2)$ is the charge relaxation resistance, and the electrochemical capacitance $C_\mu^{-1}=C^{-1}+(e^2D)^{-1}$ is the series combination of the geometrical capacitance and the density of states.[17] We assumed $C_A=C_B=C$.

In the experiment,[1] two probes are connected to a voltmeter which ideally has infinite impedance. The voltage at a lead connected to the voltmeter fluctuates to maintain zero net current. These voltage fluctuations give rise to fluctuations of the internal potentials which in turn leads to additional dephasing. For the interferometer shown in Fig. 1, this new contribution to the dephasing rate turns out to depend strongly on the probe configuration. For the dephasing rates in the local (l) and the nonlocal (nl) configuration we obtain, respectively,

$$\Gamma_\phi^l= \gamma_\phi^0+ \gamma_\phi^l, \quad \gamma_\phi^l= \gamma_\phi^0\frac{(2\mathcal{T}-1)^2}{2\mathcal{T}(1-\mathcal{T})+T_0}, \quad (5a)$$

$$\Gamma_\phi^{nl}= \gamma_\phi^0+ \gamma_\phi^{nl}, \quad \gamma_\phi^{nl}= \gamma_\phi^0\frac{(2\mathcal{T}-1)^2}{1+2T_0}. \quad (5b)$$

Here, γ_ϕ^l and γ_ϕ^{nl} are the probe-configuration specific contributions. The experiment[1] shows transmission between neighboring contacts to be significant. For better comparison, we therefore included a finite incoherent transmission $T_0=T_{12}=T_{21}=T_{34}=T_{43}$ (see Fig. 2).

The results for the dephasing rates are strongly dependent on the symmetry of the interferometer. In the symmetric case ($\mathcal{T}=1/2$) the contribution to the dephasing rate due to voltage fluctuations vanishes for both measurement configurations. Away from the symmetry point, $\mathcal{T}=1/2$, the local and the nonlocal decoherence rate differ strongly.[18] A local decoherence rate several times larger than the nonlocal one can easily be obtained for small enough T_0. The ratio of the decoherence rates for the two-probe configurations is shown in Fig. 2 as a function of the transmission probability $\mathcal{T}$.

To derive the results presented in Eqs. (5a) and (5b), we need to know the spectral function $\Sigma_{UU}(0)$ for the two different probe configurations. To start with, we want to express the Fourier transform $\Delta U(\omega)=\Delta U_A(\omega)-\Delta U_B(\omega)$ of the fluctuations of the internal potential operator through the operators for the bare charge $\Delta Q_i^b(\omega)$ ($i=A,B$) and current $\Delta I_\alpha^b(\omega)$ ($\alpha=1,\ldots,4$) fluctuations in the sample. For these quantities it is known how to calculate the spectral functions. The notation $\Delta O=O-\langle O\rangle$ denotes deviations of an operator O from its expectation value. There are two independent equations relating charge and potential fluctuations, namely,

$$\Delta Q_i = C\Delta U_i=\Delta Q_i^b-e^2D\Delta U_i+e^2\sum_\alpha D_\alpha^{(i)}\Delta V_\alpha. \quad (6)$$

Here, $\Delta Q_i^b(\omega)$ are the charge fluctuations at constant voltage and internal potential, and $\Delta V_\alpha(\omega)$ are the voltage fluctuations at contact α. The response to a change in the applied voltage at contact α is determined by the average injectivity $D_\alpha^{(i)}(\omega)=\langle D_{\alpha\alpha}^{(i)}(\omega)\rangle=\partial\langle Q_i\rangle/e^2\partial V_\alpha$. The term with the negative sign in Eq. (6) is the screening charge induced in response to a change in the internal potential. In the Thomas-Fermi approximation, the response function is the density $D(\omega)=-\partial\langle Q_i\rangle/e^2\partial U_i$. For zero frequency, we find $D=\Sigma_\alpha D_\alpha^{(i)}=4L/hv_F$ as a consequence of gauge invariance. The injectivities are the diagonal elements of the local density of states matrix[19,20] which is related to the scattering matrix $S_{\alpha\beta}$ of the system. In the zero-frequency limit

$$D_{\alpha\beta}^{(i)}(E)= -\frac{1}{2\pi i}\sum_\gamma S_{\gamma\alpha}^\dagger(E)\frac{dS_{\gamma\beta}(E)}{edU_i} \quad (7)$$

with $i=A,B$ and $\alpha,\beta,\gamma=1,\ldots,4$. The scattering matrix for the electronic interferometer can be derived using Eq. (1) (see also Ref. 12).

The voltage fluctuations entering Eq. (6) are related to the current fluctuations ΔI_α through[21]

$$\Delta I_\alpha = \Delta I_\alpha^b + \sum_\beta G_{\alpha\beta} \Delta V_\beta. \qquad (8)$$

In this Langevin-like equation, ΔI_α^b are the bare current fluctuations and $G_{\alpha\beta} = G_0(M_\alpha \delta_{\alpha\beta} - \langle T_{\alpha\beta} \rangle)$ are elements of the conductance matrix ($\alpha, \beta = 1, \ldots, 4$). For the MZI we have $M_\alpha = 1 + T_0$, where T_0 is the incoherent transmission between neighboring external leads at the same intersection. The probabilities for coherent transmission are $T_{\alpha\beta} = |S_{\alpha\beta}|^2$. The central new ingredient in this paper are the boundary conditions imposed on the voltage fluctuations ΔV_α and the fluctuations of the total currents ΔI_α by the external measurement circuit. These boundary conditions depend on the measurement configuration. In the *local configuration* (see Fig. 1) we choose contacts 1 and 4 as the current probes (they exhibit no voltage fluctuations: $\Delta V_1 = \Delta V_4 = 0$) while contacts 2 and 3 are the voltage probes (no current fluctuations: $\Delta I_2 = \Delta I_3 = 0$). In the *nonlocal configuration*, on the other hand, the voltage probes are contacts 3 and 4 (cf. Fig. 1) and thus $\Delta V_1 = \Delta V_2 = 0$ and $\Delta I_3 = \Delta I_4 = 0$. Equation (8), together with the boundary conditions for voltages and currents, can now be used to eliminate the voltage fluctuations in Eq. (6) in favor of the fluctuations of the bare currents. The potential fluctuations ΔU can then be expressed through the fluctuations of the bare currents ΔI_α^b and charges ΔQ_i^b. The result for ΔU will be different for the local and the nonlocal configuration as a consequence of the different boundary conditions.

The spectral function of the potential fluctuations is defined through the relation $2\pi\delta(\omega + \omega')\Sigma_{UU}(\omega) = \langle \Delta U(\omega)\Delta U(\omega') + \Delta U(\omega')\Delta U(\omega)\rangle/2$. Since we now know how to express the potential fluctuations for the local and the nonlocal case through the fluctuations of the bare currents and charges, we can also express the spectral function $\Sigma_{UU}(\omega)$, through the correlators of the bare charge $\Sigma_{Q_i^b Q_k^b}(\omega)$ ($i, k = A, B$), the current correlators $\Sigma_{I_\alpha^b I_\beta^b}(\omega)$ ($\alpha, \beta = 1, \ldots, 4$), and the cross correlators $\Sigma_{Q_i^b I_\alpha^b}(\omega)$ between charges and currents. For zero frequency and in the classical limit, the correlator of the charge fluctuations ΔQ_i^b and ΔQ_k^b in arms i and k is[19,20]

$$\Sigma_{Q_i^b Q_k^b}(0) = kTh \sum_{\alpha\beta} \langle D_{\alpha\beta}^{(i)} D_{\beta\alpha}^{(k)} \rangle = \delta_{ik} kTDh/2. \qquad (9)$$

The second equation is obtained from Eq. (7) and the scattering matrix of the interferometer (see Ref. 12). Finally, the current correlation functions are given by the generalized Nyquist formula,[21] $\Sigma_{I_\alpha^b I_\beta^b}(0) = kT(G_{\alpha\beta} + G_{\beta\alpha})$, while cross correlations between fluctuations of the bare charge in arm i and current fluctuations at contact α vanish $[\Sigma_{Q_i^b I_\alpha^b}(0) = 0]$ because of the absence of backscattering in our model.

We are now in a position to calculate the spectrum of the potential fluctuations in the zero-frequency limit. In the local configuration we obtain

$$\Sigma_{UU}^l(0) = 4kTR_q\left(\frac{C_\mu}{C}\right)^2\left[1 + \frac{(2T - 1)^2}{T_0 + \langle T_{13}\rangle}\right]. \qquad (10)$$
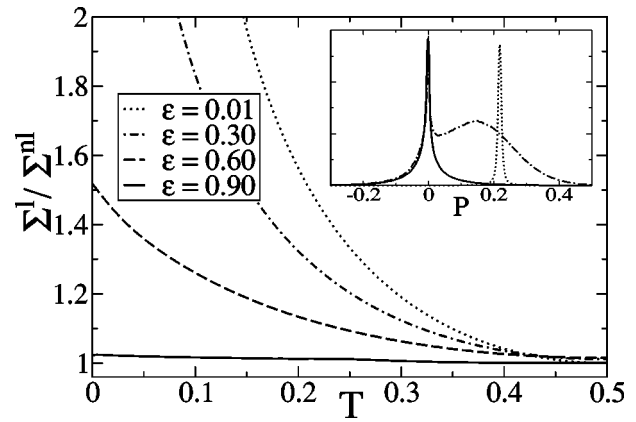

FIG. 3. Ratio of the local to the nonlocal potential fluctuation spectrum as a function of the transmission probability T at the beam splitters for different values of ε. The parameter ε controls the admixture of chaotic scattering. All curves are symmetric around $T = 1/2$. The inset shows the distribution of $P = (\Sigma_{UU}^l - \Sigma_{UU}^{nl})/(\Sigma_{UU}^{nl} + \Sigma_{UU}^l)$ for different values of ε and for $T = 0.2$.

The factor in the rectangular brackets in Eq. (10) can be understood as an enhancement of the charge relaxation resistance R_q. Attaching a voltmeter and thus closing some exits of the MZI will render charge relaxation more difficult. From comparison with Eqs. (2) and (3), it becomes clear that Eq. (10) is a self-consistent equation for the dephasing rate. In the limit of weak decoherence, the transmission probability entering Eq. (10) is flux dependent. In contrast, for the limit of strong decoherence, we can neglect the flux dependence of $\langle T_{13}\rangle$ in Eq. (10). Using Eq. (3), we then obtain the local dephasing rate, Eq. (5a). In the nonlocal case, the spectral function is independent of the magnetic field even when dephasing is weak. It is given by $\Sigma_{UU}^{nl}(0) = (2\hbar^2/e^2)\Gamma_\phi^{nl}$, leading to the dephasing rate for the nonlocal configuration, Eq. (5b).[22]

In the MZI, the intersections between contacts and arms are described by ideal beam splitters [see Eq. (1)]. Backscattering was included only through the incoherent transmission T_0 between neighboring contacts. Ideal beam splitters are rarely realized in an experiment where it is probable that scattering in the intersections exhibits a certain degree of randomness. For better comparison with the experimental situation, we now investigate numerically a model that interpolates between the ideal beam splitter and fully random scattering. The corresponding scattering matrix for one intersection is

$$\mathbf{S} = \sqrt{1-\varepsilon}\,\mathbf{S}_B - \varepsilon\mathbf{S}_B\mathbf{S}_C[1 - \sqrt{1-\varepsilon}\,\mathbf{S}_B\mathbf{S}_C]^{-1}\mathbf{S}_B, \qquad (11)$$

where $\mathbf{S}_B$ is given in Eq. (1) and $\mathbf{S}_C$ is a random matrix chosen from the circular orthogonal ensemble.[23] The parameter ε controls the admixture of chaos, $\varepsilon = 0$ corresponds to the ideal beam splitter, while $\varepsilon = 1$ corresponds to completely random scattering. In Fig. 3, the ratio of local to nonlocal potential fluctuations is shown for different values of the parameter ε. The results given there are valid in the limit of strong dephasing (as in Fig. 2) and include an ensemble average over the random matrices $\mathbf{S}_C$ of the two in-

tersections. From Fig. 3 it is clear that increasing the degree of chaotic scattering in the intersections suppresses the difference between the local and the nonlocal configuration. Backscattering, on the ensemble average, thus has a similar effect as an incoherent parallel transmission T_0 between neighboring contacts. In the limit where the intersections are fully chaotic ($\varepsilon = 1$), there is no difference between the local and the nonlocal configuration. Ensemble averaging makes the ring symmetric to any measurement configuration.

The ratio of the fluctuation spectra is of course strongly sample specific. This point is emphasized in the upper inset of Fig. 3 where the distribution of the quantity $P = (\Sigma_{UU}^l - \Sigma_{UU}^{nl})/(\Sigma_{UU}^l + \Sigma_{UU}^{nl})$ is shown for different values of ε and for $T = 0.2$. For weak disorder ($\varepsilon = 0.01$, dotted curve), P almost always takes the value expected for an ideal beam splitter whereas for strong disorder ($\varepsilon = 0.9$, full line) the distribution of P is roughly symmetric around $P = 0$. Still, there is a good chance to find a sample where $P \neq 0$ and thus the local and nonlocal fluctuation spectra differ from each other. Finally, in the intermediate case ($\varepsilon = 0.3$, dashed-dotted line) the distribution interpolates between the two limiting cases.

In the experiment,[1] the four-terminal resistance $R_{\alpha\beta,\gamma\delta} = (V_\gamma - V_\delta)/I_\alpha$ with $I_\beta = -I_\alpha$ was measured. In terms of the conductance matrix elements, the four-terminal resistances are $R_{\alpha\beta,\gamma\delta} = (G_{\gamma\alpha}G_{\delta\beta} - G_{\gamma\beta}G_{\delta\alpha})/D$,[6] where D is any sub-determinant of rank 3 of the total conductance matrix. The four-terminal resistance takes a particularly simple form in the case of a reflectionless interferometer ($\varepsilon = 0$) where we find

$$R_{14,23} = \frac{h}{2e^2} \frac{T_0 - \langle T_{13} \rangle}{1 + T_0 - \langle T_{13} \rangle}, \tag{12a}$$

$$R_{12,43} = \frac{h}{2e^2} \frac{1 - 2\langle T_{13} \rangle}{(T_0 + \langle T_{13} \rangle)(1 + T_0 - \langle T_{13} \rangle)} \tag{12b}$$

for the local and the nonlocal configuration, respectively. Equations (12a) and (12b) show that the attenuation of the local and nonlocal resistances is determined by the decoherence rates Eqs. (5a) and (5b) respectively.

In conclusion, we have shown that the electrical constraints imposed by the measurement circuit give rise to a probe-configuration dependence of the dephasing rate. This effect is most pronounced in an ideal quantum interferometer that is strongly asymmetric, but was found to persist even in the presence of a considerable admixture of incoherent transmission or randomness (with ensemble averaging). While there may be other physical mechanisms for producing such a difference, our discussion of dephasing explicitly includes the effect of the external electrical circuit and leads to a result consistent with unanticipated experimental observations.

[1] K. Kobayashi, H. Aikawa, S. Katsumoto, and Y. Iye, J. Phys. Soc. Jpn. **71**, 2094 (2002).

[2] Y. Aharonov and D. Bohm, Phys. Rev. **115**, 485 (1959).

[3] B.L. Altshuler, A.G. Aronov, and D. Khmelnitskii, J. Phys. C **15**, 7367 (1982).

[4] M.H. Devoret, D. Esteve, H. Grabert, G.-L. Ingold, H. Pothier, and C. Urbina, Phys. Rev. Lett. **64**, 1824 (1990).

[5] C.W.J. Beenakker, M. Kindermann, and Yu.V. Nazarov, Phys. Rev. Lett. **90**, 176802 (2003).

[6] M. Büttiker, Phys. Rev. Lett. **57**, 1761 (1986).

[7] C.P. Umbach, P. Santhanam, C. van Haesendonck, and R.A. Webb, Appl. Phys. Lett. **50**, 1289 (1987).

[8] U.F. Kayser, S. Borck, R.J. Haug, M. Bichler, G. Abstreiter, and W. Wegscheider, Semicond. Sci. Technol. **17**, L22 (2002).

[9] Y. Ji, Y. Chung, D. Sprinzak, M. Heiblum, D. Mahalu, and H. Shtrikman, Nature (London) **422**, 415 (2003).

[10] M. Cassé, Z.D. Kvon, G.M. Gusev, E.B. Olshanetskii, L.V. Litvin, A.V. Plotnikov, D.K. Maude, and J.C. Portal, Phys. Rev. B **62**, 2624 (2000).

[11] A.E. Hansen, A. Kristensen, S. Pedersen, C.B. Sørensen, and P.E. Lindelof, Phys. Rev. B **64**, 045327 (2001).

[12] G. Seelig and M. Büttiker, Phys. Rev. B **64**, 245313 (2001).

[13] J.P. Bird, K. Ishibashi, D.K. Ferry, Y. Ochiai, Y. Aoyagi, and T. Sugano, Phys. Rev. B **51**, 18 037 (1995); D.P. Pivin, Jr., A. Andresen, J.P. Bird, and D.K. Ferry, Phys. Rev. Lett. **82**, 4687 (1999); C. Prasad *et al.*, Phys. Rev. B **62**, 15 356 (2000).

[14] R.M. Clarke, I.H. Chan, C.M. Marcus, C.I. Duruöz, J.S. Harris, Jr., K. Campman, and A.C. Gossard, Phys. Rev. B **52**, 2656 (1995); A.G. Huibers, M. Switkes, C.M. Marcus, K. Campman, and A.C. Gossard, Phys. Rev. Lett. **81**, 200 (1998); A.G. Huibers, J.A. Folk, S.R. Patel, C.M. Marcus, C.I. Duruöz, and J.S. Harris, Jr., *ibid.* **83**, 5090 (1999).

[15] Y. Takane, J. Phys. Soc. Jpn. **67**, 3003 (1998); **71**, 2617 (2002).

[16] AB oscillations in a MZI with two arms of equal length are not affected by thermal averaging.

[17] M. Büttiker, H. Thomas, and A. Prêtre, Phys. Lett. A **180**, 364 (1993).

[18] If $T_0 = 0$, the local dephasing rate, Eq. (5a) diverges for $\mathcal{T} = 0$ and $\mathcal{T} = 1$. The divergence has its origin in the fact that for $\mathcal{T} = 0$ and $\mathcal{T} = 1$ the two arms of the MZI become decoupled. It is therefore cutoff by any backscattering.

[19] M.H. Pedersen, S.A. van Langen, and M. Büttiker, Phys. Rev. B **57**, 1838 (1998).

[20] A.M. Martin and M. Büttiker, Phys. Rev. Lett. **84**, 3386 (2000).

[21] M. Büttiker, Phys. Rev. B **46**, 12 485 (1992).

[22] The results, Eqs. (5a) and (5b), and (10) can also be extracted from the self-consistent admittance matrix (Ref. 12) if the appropriate boundary conditions are used [A. N. Jordan (unpublished)].

[23] P.W. Brouwer and C.W.J. Beenakker, J. Math. Phys. **37**, 4904 (1996).